Theoretical and experimental evidence of negative refraction of water waves in elliptic and hyperbolic regimes

A. Maurel[a], L.P. Euvé[b], P. Petitjeans[b], V. Pagneux[c], K. Pham[d]

[a]ESPCI Paris, PSL University, CNRS, Institut Langevin, France
[b]ESPCI Paris, PSL University, CNRS, PMMH, France
[c]LAUM, Le Mans, France
[d]ENSTA Paris, LMI, Institut Polytechnique de Paris, 91120, Palaiseau, France

email : agnes.maurel@espci.fr

1 INTRODUCTION

Metamaterials push the boundaries of wave control by enabling the exploitation of unusual physical properties such as negative refraction and extreme anisotropy. In the context of surface water waves, these advances pave the way for innovative applications, transforming propagation characteristics through specially designed resonant systems (see the recent review in [1]). This work investigates unconventional wave propagation phenomena on water surfaces using metamaterials designed to alter their dispersion. On one hand, elliptical dispersion with double negativity is achieved through a system of underwater resonant cavities, demonstrating both positive and negative refractive indices depending on the regime [2]. On the other hand, hyperbolic dispersion is realized in devices combining open channels with subwavelength resonators, resulting in an effective negative water depth and negative refraction [3, 4]. Together, these studies highlight innovative mechanisms for wave manipulation, bridging concepts of double negativity and hyperbolic dispersion with the properties of water-wave metamaterials.

(a) elliptic (b) hyperbolic

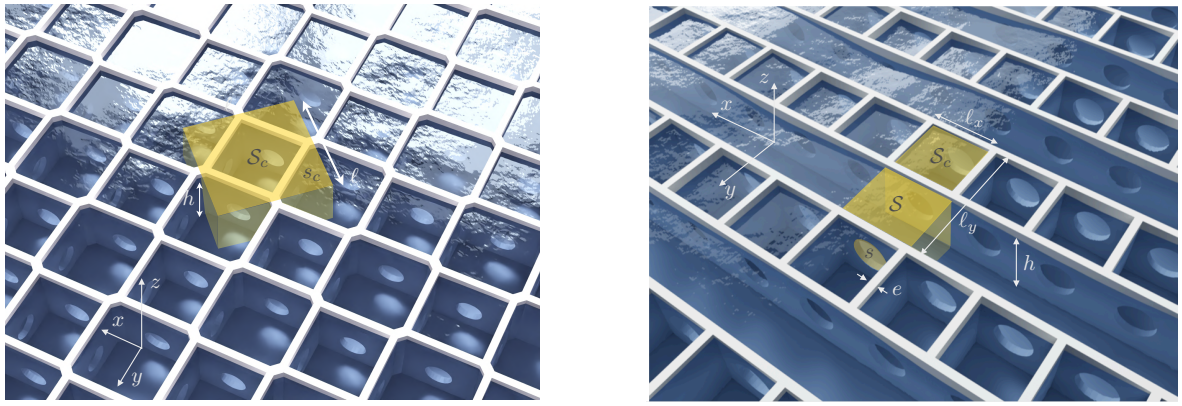

Figure 1: Conceptuel views of the arrays of resonant cavities realizing metamaterials for water waves with (a) elliptic dispersion and (b) hyperbolic dispersion with negative refraction. The highlighted regions show the 3D unit cells.

2 THEORETICAL ANALYSIS

Water waves propagate along the free surface of a water column. Under the assumptions of an inviscid, incompressible fluid with irrotational motion, the velocity field $\boldsymbol{U}(\boldsymbol{r}, z)$, where $\boldsymbol{r} = (x, y)$ denotes the horizontal coordinates, and its associated velocity potential $\Phi(\boldsymbol{r}, z)$ satisfy

$$\mathrm{div}\boldsymbol{U} = 0, \quad \boldsymbol{U} = \nabla\Phi, \quad U_z(\boldsymbol{r}, 0) = \frac{\omega^2}{g}\Phi(\boldsymbol{r}, 0), \quad \boldsymbol{U}\cdot\boldsymbol{n} = 0 \text{ on the walls}, \tag{1}$$

where U_z is the vertical velocity component, ω is the angular frequency, and g represents gravity. For a water column with constant depth h, waves follow the dispersion relation $\omega^2 = gk\tanh(kh)$. In the presence of resonant cavities (figure 1(a) or (b)), the analysis follows the asymptotic approach developed in [3, 4], assuming that the size of the cavities and the water depth are small compared to the reference wavelength $1/k$.

In this framework, the potential inside the cavities is constant, and communication between cavities occurs locally at their openings through incoming and outgoing fluxes. A detailed analysis of the flow in the openings shows that the velocity is constant there, so the flux entering cavity 2 from cavity 1 is given by $F = \alpha(\varphi_2 - \varphi_1)$, with $\alpha = s/e$, where s is the cross-sectional area and e is the effective length of the hole, accounting for boundary layer effects. Applying Bloch-Floquet conditions across the array and integrating the incompressibility condition over the volume of each cavity in the unit cell reveals the dynamic boundary conditions at the free surface and the contribution of fluxes between communicating regions. We obtain:

$$\Phi(\boldsymbol{r}, z) = \varphi(\boldsymbol{r}), \quad \varphi(\boldsymbol{r}) = \varphi e^{i\kappa_x x + i\kappa_y y}, \tag{2}$$

where φ is piecewise constant within each cavity in the unit cell.

Elliptic dispersion with double negativity – For this configuration, we use (2) in the larger cavity with horizontal cross-section S_c ($\varphi = \varphi_1$) and in the smaller one with cross-section s_c ($\varphi = \varphi_2$). By doing so, we find the system reads

$$\begin{cases} (\Omega^2 - 1)\varphi_1 + e^{-i(\kappa_x+\kappa_y)\ell/2}\,\cos\dfrac{\kappa_x\ell}{2}\cos\dfrac{\kappa_y\ell}{2}\,\varphi_2 = 0, \\ \left(\Omega^2 - \gamma\right)\varphi_2 + \gamma e^{i(\kappa_x+\kappa_y)\ell/2}\,\cos\dfrac{\kappa_x\ell}{2}\cos\dfrac{\kappa_y\ell}{2}\,\varphi_1 = 0, \end{cases} \tag{3}$$

where $\Omega = \omega/\omega_\mathrm{c}$ and $\omega_\mathrm{c}^2 = 4g\alpha/S_\mathrm{c}$ and $\gamma = S_\mathrm{c}/s_\mathrm{c}$. The solvability condition of (3) provides the dispersion relation $\boldsymbol{\kappa}(\Omega)$, of the form

$$\cos^2\frac{\kappa_x\ell}{2}\cos^2\frac{\kappa_y\ell}{2} = \frac{1}{\gamma}\left(\Omega^2 - 1\right)\left(\Omega^2 - \gamma\right). \tag{4}$$

The corresponding full band structure is shown in figure 2(a) for $\gamma = 2$, revealing two passbands for $\Omega \in (0, 1)$ and $\Omega \in (\sqrt{\gamma}, \sqrt{\gamma+1})$. This latter is associated with negative group velocity. In particular close to $\Omega = \sqrt{\gamma+1}$, the propagation is isotropic, with $V_\mathrm{g} = \partial_\kappa\omega$ given by

$$V_\mathrm{g} = -\frac{\omega_\mathrm{c}\ell}{2}\sqrt{\frac{\gamma}{\gamma+1}\left(1 - \frac{\Omega^2}{\gamma+1}\right)} \leq 0. \tag{5}$$

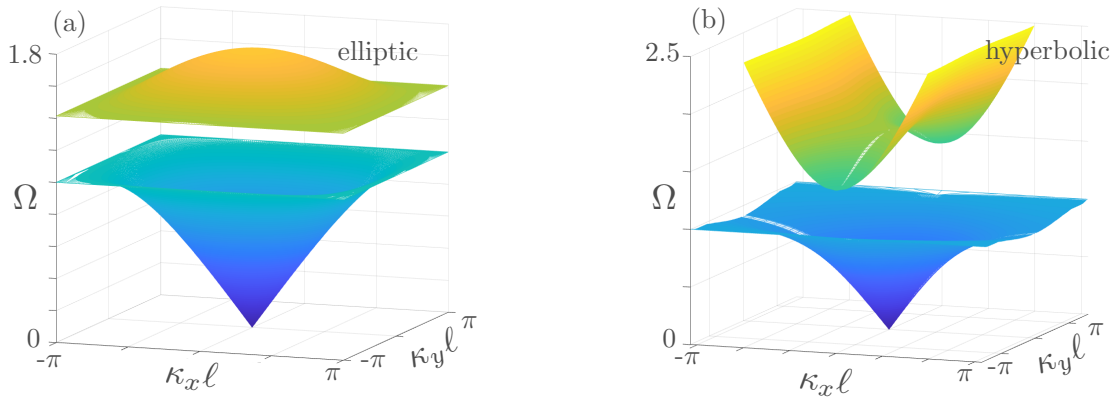

Figure 2: Theoretical full band structure $\boldsymbol{\kappa}$ as a function of the non dimensional frequency Ω.

Hyperbolic dispersion – A similar analysis applies to the structure of figure 1(b), see [3], in the close cavity with horizontal cross-section S_c ($\varphi = \varphi_1$) and in the open avenue with cross-section S ($\varphi = \varphi_2$), resulting in

$$\begin{cases} (\Omega^2 - 1)\varphi_1 + e^{-i\kappa_y \ell_y/2} \cos\dfrac{\kappa_y \ell}{2}\, \varphi_2 = 0, \\ \left((\Omega^2 - \gamma) - \dfrac{\kappa_x^2}{\kappa_c^2}\right) \varphi_2 + \gamma e^{i\kappa_y \ell_y/2} \cos\dfrac{\kappa_y \ell}{2}\, \varphi_1 = 0, \end{cases} \tag{6}$$

where $\Omega = \omega/\omega_c$ and $\omega_c^2 = 2g\alpha/S_c$, $\gamma = S_c/S$ and $\kappa_c = \gamma\omega_c/(gh)$. Again, the solvability condition of (6) provides the dispersion relation of the form

$$(\Omega^2 - 1)\frac{\kappa_x^2}{\kappa_c^2} + \cos^2\frac{\kappa_y \ell}{2} = \frac{1}{\gamma}(\Omega^2 - 1)\left(\Omega^2 - \gamma\right). \tag{7}$$

The full band structure (figure 2(b)) reveals two pass-bands for $\Omega \in (0, 1)$ and $\Omega \in (\sqrt{\gamma}, +\infty)$ (compared to the first structure, the propagation for large Ω is allowed thanks to the free propagation in the avenues). The second pass-band has hyperbolic type dispersion and, near the saddle point at $\Omega = \sqrt{\gamma + 1}$ where $\kappa_y \ell \ll 1$, the dispersion (7) reads

$$\frac{\kappa_x^2}{\kappa_c^2} - \frac{\kappa_y^2 \ell^2}{4\gamma} = \left(\frac{\gamma + 1}{\gamma}\right)^2 \left(\frac{\Omega^2}{\gamma + 1} - 1\right), \tag{8}$$

which is hyperbolic with major axis along κ_y (resp. along κ_x) below (resp. above) the saddle point.

3 Experimental set-up and results

We experimentally validated the dispersion relations (4) and (7) (results will be presented). Below we report the experimental results demonstrating the potential for negative refraction in the metamaterials. The cavities were fabricated using a 3D printer with a resin material that allows the menisci to slide smoothly along the walls. Their dimensions are as follow:

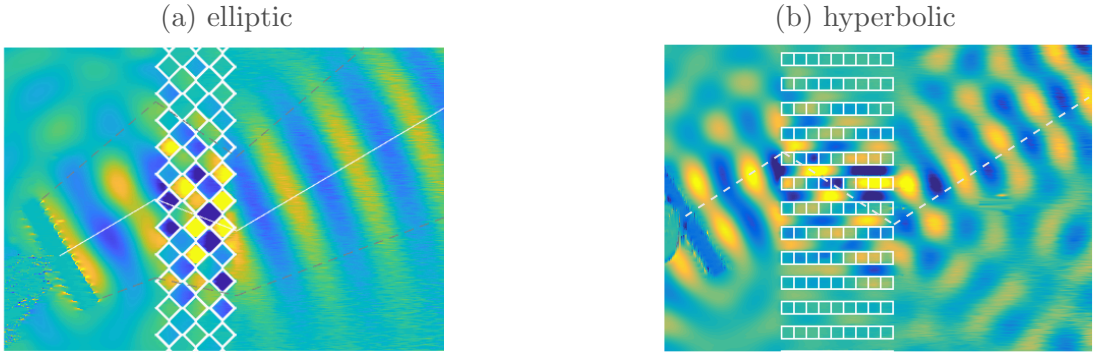

Figure 3: Experimental evidence of negative refraction in (a) the elliptic metamaterial with double negativity and (b) the hyperbolic metamaterial. The plain/dashed lines show the theoretical trajectories of the beam from (4) and (7).

both cases $h = 2$ cm, and we used (a) a unit cell dimension of $\ell^2 \times h$ with $\ell = 2/\sqrt{2}$ cm^2, $S_c = 6.2$ cm^2, $s_c = 4.4$ cm^2 and (b) a unit cell dimension $\ell_x \times \ell_y \times h$, $\ell_x = 2$ cm, $\ell_y = 4$ cm, $S_c = 1.8^2$ cm^2, $S = 1.8 \times 2$ cm^2.

We used an incident beam generated by an oscillating cylinder, 16 cm long (approximatively 2 wavelengths) and 4 cm in diameter driven by a linear motor, which strikes an interface with a metamaterial slab at an angle of $\theta^{\text{in}} \simeq 30°$ to the normal of the interface. The working frequencies are about 4 Hz, in the second passband, where the refraction was determined to be negative. Figures 3 show the displacement field measured by FTP, with losses compensated. In both cases, negative refraction is visible to the naked eye, with a beam emerging from the slab shifted downward compared to the incident beam. This observation agrees with the theoretical trajectories shown by the solid and dashed lines. These trajectories were obtained by using (4) and (7), along with the conservation of the wave vector component along y and the causality condition, which ensures that the energy flux has a positive component in the x-direction.

REFERENCES

[1] Zhu, S., Zhao, X., Han, L., Zi, J., Hu, X., and Chen, H. 2024. *Controlling water waves with artificial structures.* Nature Reviews Physics 6(4), 231–245.

[2] Euvé, L.-P., Pham, K., Petitjeans, P., Pagneux, V., and Maurel, A. *Experimental evidence of negative refraction index in a metamaterial for water waves. submitted.*

[3] Euvé, L.-P., Pham, K., and Maurel, A. 2023. *Negative refraction of water waves by hyperbolic metamaterials. Journal of Fluid Mechanics 961*, A16.

[4] Euvé, L.-P., Pham, K., Petitjeans, P., Pagneux, V., and Maurel, A. 2024. *Experimental demonstration of negative refraction of water waves using metamaterials with hyperbolic dispersion.* Physical Review Fluids 9(11), L112801.